This is an open access article published under a Creative Commons Attribution (CC-BY) License, which permits unrestricted use, distribution and reproduction in any medium, provided the author and source are cited.

ACS OMEGA

Article

Cite This: ACS Omega 2019, 4, 13981−13990

http://pubs.acs.org/journal/acsodf

Investigating the Acid Site Distribution of a New-Generation Methyl Chloride Synthesis Catalyst

Alastair R. McInroy,[†] John M. Winfield,[†] Christopher C. Dudman,[‡] Peter Jones,[‡] and David Lennon*,[†]

[†]School of Chemistry, Joseph Black Building, University of Glasgow, Glasgow G12 8QQ, U.K.

[‡]Inovyn, South Parade, Runcorn, Cheshire WA7 4JE, U.K.

Supporting Information

ABSTRACT: The effect of modifying an η-alumina methyl chloride synthesis catalyst by doping with CsCl and KCl over the concentration range of 0.1−1.0 mmol $g_{(cat)}^{-1}$ is investigated by a combination of pyridine chemisorption coupled with infrared spectroscopy and mass-selective temperature-programmed desorption measurements. The loading of group 1 metal chloride is equivalent to a titrant that enables selective neutralization of Lewis acid sites present at the surface of the reference η-alumina catalyst. Specifically, a loading of 0.1 mmol $g_{(cat)}^{-1}$ is sufficient to neutralize the strong Lewis acid sites; a loading of 0.6 mmol $g_{(cat)}^{-1}$ is sufficient to neutralize the strong and medium-strong Lewis acid sites; a loading of 1.0 mmol $g_{(cat)}^{-1}$ neutralizes all of the strong and medium-strong Lewis acid sites and partially neutralizes the medium-weak Lewis acid site. These deductions connect with a catalyst design program to develop a methyl chloride synthesis catalyst that exhibits minimal formation of the byproduct dimethyl ether.

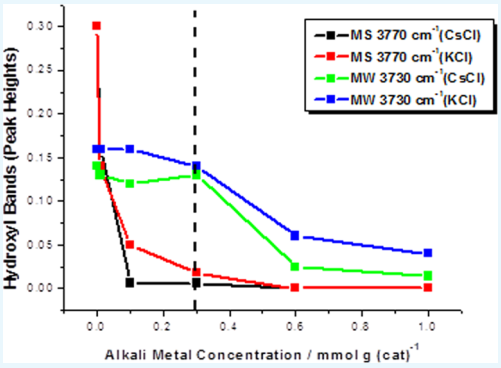

1. INTRODUCTION

Methyl chloride is an important chemical compound: in 1997, productions within the regions of United States, western Europe, and Japan were 0.51, 0.48, and 0.14 Mton, respectively.[1] The global chloromethane market is expected to garner $2171.6 million by 2022, with the market exhibiting a compound annual growth rate of 4.63% over the period 2016−2022.[2] Methyl chloride is used for the methylation of phenols, alcohols, and cellulose. It is also used in the manufacture of methylchlorosilanes (precursors to silicones) and quaternary ammonium salts.[1] Two principal routes dominate the industrial-scale manufacture of methyl chloride: (i) methane chlorination and (ii) the esterification of methanol with anhydrous hydrogen chloride. The latter route is performed in the liquid or gaseous phase and may involve catalysts such as $ZnCl_2$, $CuCl_2$, H_3PO_4, or Al_2O_3. Presently, the hydrochlorination of methanol is thought to be the most important commercially exploited route to methyl chloride;[1] this article examines aspects of the surface chemistry of this process over η-alumina-based catalysts

$$CH_3OH + HCl \rightarrow CH_3Cl + H_2O \quad (1)$$

$$2\ CH_3OH \rightarrow CH_3OCH_3 + H_2O \quad (2)$$

eq 1 describes methyl chloride synthesis from the reaction between methanol and anhydrous hydrogen chloride, with the reaction thought to be favored over Lewis acid sites.[3] Selectivity to methyl chloride is reduced by the reaction shown in eq 2, where the alcohol is converted to dimethyl ether. The reactions shown in eqs 1 and 2 are both reversible; so, at any given feed composition and temperature, there is an equilibrium product composition. An improved methyl chloride synthesis catalyst will catalyze reaction 1 more effectively than reaction 2.

Schmidt and co-workers have examined methyl chloride synthesis via the hydrochlorination of methanol over a range of materials. Representative studies include the use of microreactors[4,5] and the use of $ZnCl_2$-modified zeolite and alumina-based catalysts.[6,7] The latter work illustrates how the addition of a zinc salt can modify the acid properties of a γ-alumina catalyst to beneficially influence product yields.

Following a series of investigations connected with the use of η-Al_2O_3 as a methyl chloride synthesis catalyst,[3,8−16] in 2016, McInroy and co-workers proposed a mechanism for methyl chloride production over this material.[17] Furthermore, as part of an academic/industrial collaboration, the work additionally considered a role for chemical modifiers to improve product selectivity. This was in response to an industrial driver to reduce the quantities of dimethyl ether in the product stream. The formation of dimethyl ether during methyl chloride production is problematical in the industrial operation, as the byproduct can react with chlorine elsewhere in the chloromethane production process to produce undesirable chlorinated ethers.[17] Thus, from the industrial perspective, enhanced methyl chloride selectivity is the primary objective.

Received: June 11, 2019
Accepted: July 30, 2019
Published: August 12, 2019

Downloaded via UNIV OF GLASGOW on September 12, 2019 at 13:50:07 (UTC).
See https://pubs.acs.org/sharingguidelines for options on how to legitimately share published articles.

The 2016 study by McInroy et al. showed how the addition of group 1 metal salts to the well-characterized η-alumina catalyst could lead to commercially significant improvements in product selectivity.[17] Specifically, the doping of the η-alumina reference catalyst with CsCl and KCl in the range of 0−1.0 mmol $g_{(cat)}^{-1}$ attenuated dimethyl ether formation. For example, although the doping of the η-alumina catalyst leads to a reduction in the rate of CH_3Cl formation (1.0 mmol CsCl $g_{(cat)}^{-1}$ reduces the production rate for CH_3Cl at 560 K by 57%), it nevertheless significantly improves the product selectivity (1.0 mmol CsCl $g_{(cat)}^{-1}$ increases the methyl chloride selectivity at 563 K from 94.5 to 99.6%). On balance, CsCl doping at a loading of ≥0.3 mmol $g_{(cat)}^{-1}$ was considered to represent the best catalyst formulation for a sustained CH_3Cl production with minimal formation of CH_3OCH_3, where the kinetic control of the product composition was possible.[17] Concerning the origins for these improvements in catalytic performance, and with reference to previous characterization studies,[10] it was surmised that the group 1 salts were "capping" the strong and medium-strong (MS) Lewis acid sites of the η-alumina catalyst and that methyl chloride production was occurring solely on medium-weak (MW) Lewis acid sites.[17]

The present communication explores the matter of the acid site distribution present on the η-alumina catalyst[18] and uses pyridine as a probe molecule to discern how the group 1 metal salts within the designated concentration range moderate the distribution of the η-alumina Lewis acid sites to yield a more selective methyl chloride synthesis catalyst. A combination of pyridine chemisorption, infrared spectroscopy, and temperature-programmed desorption is adopted throughout, enabling a site-selective model to be proposed that can be linked to improvements in catalytic performance. The use is made of a previously reported four-site surface structural model for η-alumina reported by Lundie and co-workers that comprises (i) strong, (ii) medium-strong, (iii) medium-weak, and (iv) weak-strength Lewis acid sites.[10] Whereas infrared spectroscopy of chemisorbed pyridine as a probe base was able to reproduce the accepted three-site model of strong, medium, and weak Lewis acid sites via the pyridine 8a ν(C−C) mode,[19,20] complementary temperature-programmed desorption experiments were able to subdivide the medium-strength Lewis acid site into medium-strong and medium-weak Lewis acid sites.[10] In combination with the 2016 publication by McInroy et al., which reports that microreactor test outcomes for group 1 metal salts modified η-alumina catalysts,[17] this article describes a component of a catalyst design process and rationalizes how certain modifications to the reference catalyst (η-alumina) can minimize byproduct formation. Thus, the work constitutes an example of industrial-scale Green Chemistry, with catalytic science being the enabling technology.[21]

2. RESULTS

2.1. IR Studies of Pyridine Adsorption Over CsCl- and KCl-Doped η-Al_2O_3 Catalysts. *2.1.1. $Py_{(ad)}$ ν(C−C) Modes.* Figure 1 presents the infrared spectrum in the region of 1700−1400 cm^{-1} of a saturated overlayer of chemisorbed pyridine as a function of CsCl doping concentration. Figure 1a represents the undoped η-alumina reference catalyst that has been comprehensively analyzed by Lundie and co-workers.[10] Concentrating on the diagnostic pyridine 8a ν(C−C) mode, bands observed at 1623, 1613, and 1595 cm^{-1} are assigned to pyridine residing in, respectively, strong, medium, and weak Lewis acid sites.[10] The pyridine 8a mode cannot delineate between medium-strong and medium-weak Lewis acid sites.[10]

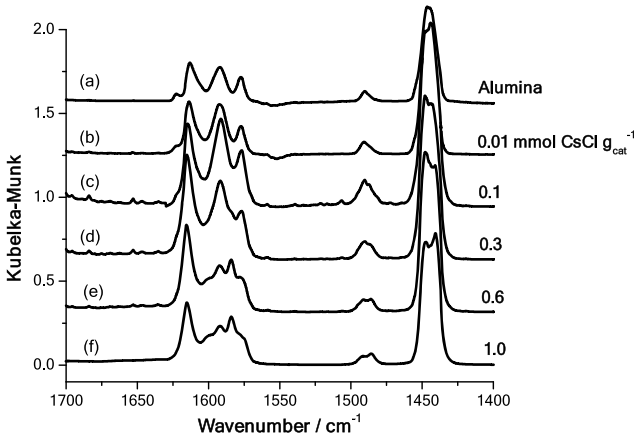

Figure 1. Infrared difference spectra for a saturated overlayer of pyridine on a range of CsCl-doped alumina catalysts: (a) undoped η-alumina, (b) 0.01 mmol CsCl $g_{(cat)}^{-1}$, (c) 0.1 mmol CsCl $g_{(cat)}^{-1}$, (d) 0.3 mmol CsCl $g_{(cat)}^{-1}$, (e) 0.6 mmol CsCl $g_{(cat)}^{-1}$, and (f) 1.0 mmol CsCl $g_{(cat)}^{-1}$. The spectra are offset for clarity.

Figure 1b−e presents the corresponding IR spectra for pyridine bound to the reference catalyst doped over the range of 0.01−1.0 mmol CsCl $g_{(cat)}^{-1}$. Although the spectral frequency of the 8a mode bandheads is unaffected by the doping process, low concentrations of CsCl result in an enhancement of signal intensity in the region of 1700−1400 cm^{-1}. As the group 1 metal salt loadings are increased further, these intensities begin to decrease. Figure 2 shows this effect

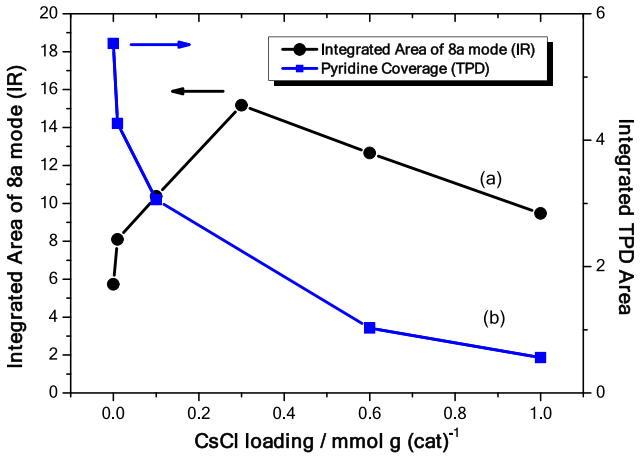

Figure 2. Correlation of (a) the integrated area of the pyridine 8a mode and (b) integrated area of pyridine TPD profiles (Section 2.3) as a function of CsCl loading. (An offset in the integrated area of the IR measurement is connected with the deconvolution of the 8a features in the spectrum.)

for the CsCl-doped catalysts by plotting the integrated area of all bands associated with the pyridine 8a mode against the CsCl concentration. The grouping of the 8a band intensities in this way is intended to indicate how the bands signifying Lewis acidity scale with respect to modifier exposure. For CsCl loadings up to 0.4 mmol CsCl $g_{(cat)}^{-1}$, there is an increase in integrated 8a intensity; thereafter, the band intensity is seen to decrease. Section 2.3 outlines a series of temperature-programmed desorption (TPD) measurements performed as

DOI: 10.1021/acsomega.9b01719
ACS Omega 2019, 4, 13981−13990

a function of group 1 metal salt loading that enables the pyridine coverage as a function of modifier loading to be determined. That information is included in Figure 2 and shows, as expected, that the surface pyridine concentration is progressively reduced on increasing CsCl loadings. Thus, Figure 2 indicates that there is an intensity enhancement effect for the pyridine 8a modes that, presumably, is related to the electronic properties of the modifier and that this effect is nonlinear with respect to pyridine coverage. This phenomenon is tentatively attributed to the group 1 metal salt by either enhancing the dynamic dipole moment of the 8a mode of chemisorbed pyridine or inducing a degree of dipole coupling within the chemisorbed overlayer of oscillators.

Figure 2 indicates that two competing factors govern the spectral intensity of the probe molecule. First, there is an enhancement effect induced by the additive but, second, this is tempered by a decrease in pyridine coverage as dopant loading increases. Inspection of Figure 2 suggests that, at dopant loadings below 0.3 mmol $g_{(cat)}^{-1}$, the enhancement effect is the greater factor, whereas above this value, the decrease in coverage outweighs any signal enhancement and a decrease in 8a intensities is observed. These competing factors mean that a direct correlation between the IR intensity of the pyridine 8a modes with respect to modifier loading is not readily achievable under these conditions.

Figure 3 presents the corresponding IR spectra for pyridine-dosed KCl catalysts, while Figure 4 presents the integrated

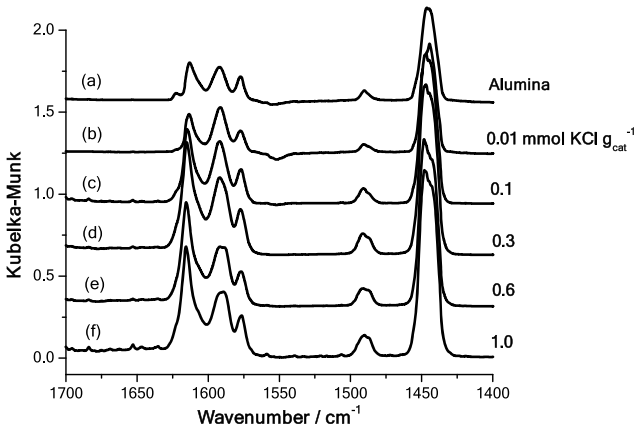

Figure 3. Infrared difference spectra for a saturated overlayer of pyridine on a range of KCl-doped alumina catalysts: (a) undoped η-alumina, (b) 0.01 mmol KCl $g_{(cat)}^{-1}$, (c) 0.1 mmol KCl $g_{(cat)}^{-1}$, (d) 0.3 mmol KCl $g_{(cat)}^{-1}$, (e) 0.6 mmol KCl $g_{(cat)}^{-1}$, and (f) 1.0 mmol KCl $g_{(cat)}^{-1}$. The spectra are offset for clarity.

pyridine 8a intensity profile as a function of KCl loadings that is additionally plotted alongside the relative TPD-derived pyridine coverage values. Trends observed for the CsCl-loaded catalysts are essentially reproduced with the KCl counterparts, most notably including the pyridine 8a mode intensity as a function of group 1 metal salt loading (Figures 2 and 4).

Despite complications arising from group 1 metal salt doping of η-alumina leading to the spectral enhancement of the 8a mode of chemisorbed pyridine, it is still possible to discern, and subsequently assign, chemically relevant spectral features evident in Figures 1 and 3. In both cases, the 8a mode at 1623 cm^{-1}, assigned to pyridine adsorbed on strong acid sites,[10] is effectively removed at loadings of 0.1 mmol $g_{(cat)}^{-1}$. Above these levels, it appears that the dopant has essentially

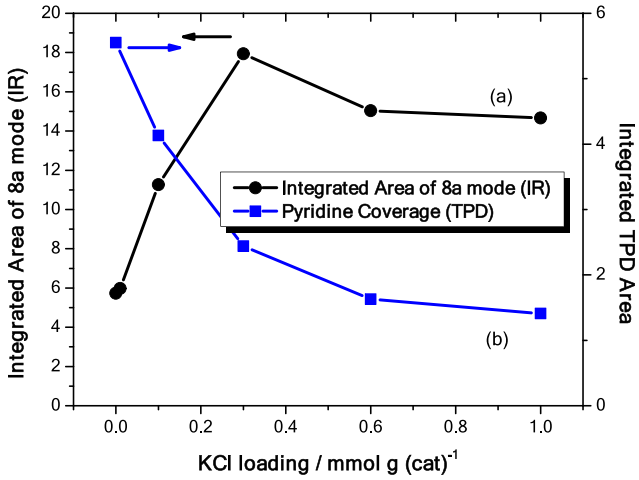

Figure 4. Correlation of (a) the integrated area of the pyridine 8a mode and (b) the integrated area of pyridine TPD profiles (see Section 2.3) as a function of KCl loading. (An offset in the integrated area of the IR measurements is connected with the deconvolution of the 8a features in the spectrum.)

"capped" all of the strong acid sites. Bands associated with medium and weak Lewis acid sites remain at all dopant loadings.

The effect of dopant loading on the medium-strength Lewis acid sites is difficult to quantify via the 8a mode, both due to the apparent enhancement effect and to the fact that medium-strong and medium-weak Lewis acid sites are indistinguishable by IR spectroscopy.[10] Certainly, some differences are evident between the profiles for the CsCl (Figure 1) and KCl (Figure 3) series. To examine these issues further, it is informative to examine the hydroxyl stretching region of the doped aluminas.

2.1.2. Alumina ν(O−H) Modes. Figures 5 and 6 show the infrared difference spectra recorded in the region between 3800 and 3650 cm^{-1} for pyridine adsorbed on the CsCl- and KCl-doped catalysts, respectively. In both cases, the infrared spectra show a series of negative bands assigned to surface hydroxyl groups interacting with pyridine adsorbed on

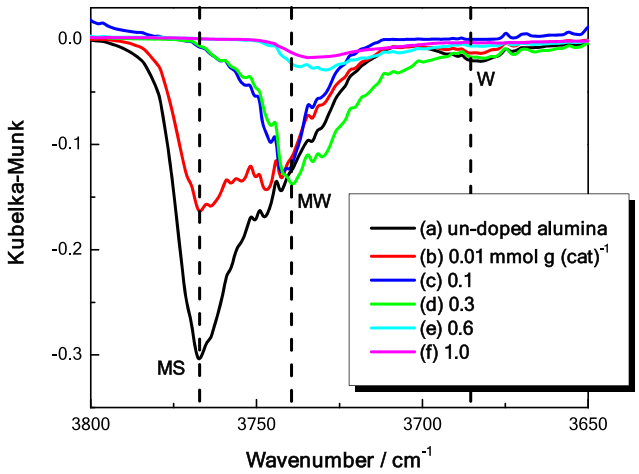

Figure 5. Infrared difference spectra of the hydroxyl stretch region for a saturated overlayer of pyridine on a range of CsCl-doped alumina catalysts: (a) undoped η-alumina, (b) 0.01 mmol CsCl $g_{(cat)}^{-1}$, (c) 0.1 mmol CsCl $g_{(cat)}^{-1}$, (d) 0.3 mmol CsCl $g_{(cat)}^{-1}$, (e) 0.6 mmol CsCl $g_{(cat)}^{-1}$, and (f) 1.0 mmol CsCl $g_{(cat)}^{-1}$.

DOI: 10.1021/acsomega.9b01719
ACS Omega 2019, 4, 13981−13990

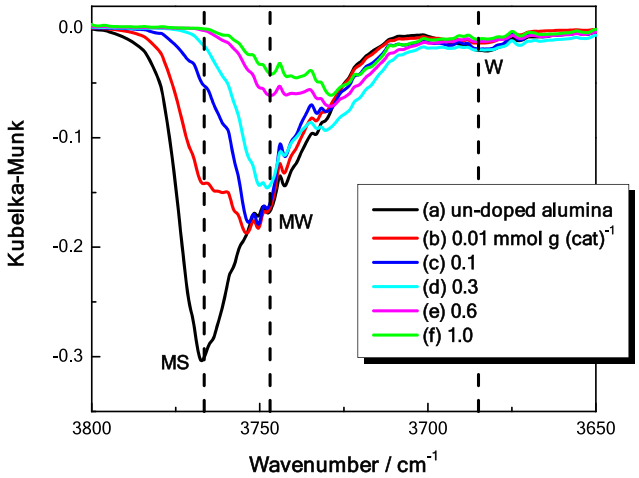

Figure 6. Infrared difference spectra of the hydroxyl stretch region for a saturated overlayer of pyridine on a range of KCl-doped alumina catalysts: (a) undoped η-alumina, (b) 0.01 mmol KCl $g_{(cat)}^{-1}$, (c) 0.1 mmol KCl $g_{(cat)}^{-1}$, (d) 0.3 mmol KCl $g_{(cat)}^{-1}$, (e) 0.6 mmol KCl $g_{(cat)}^{-1}$, and (f) 1.0 mmol KCl $g_{(cat)}^{-1}$.

medium-strong, medium-weak, and weak Lewis acid sites as signified by bands at 3770, 3730, and 3690 cm^{-1}, respectively.[10] It is worthwhile noting that the strong Lewis acid site is a coordinatively unsaturated aluminum ion with no "partner" hydroxyl group;[10] thus, this site has no signature in the hydroxyl stretching region of the spectrum. The spectral intensities of the medium-strong and medium-weak sites as a function of CsCl and KCl loadings are presented in Figure 7,

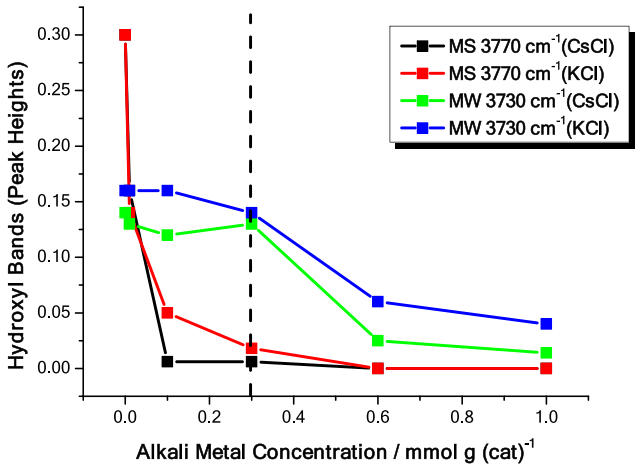

Figure 7. Peak heights of hydroxyl bands associated with the medium-strong (MS) and medium-weak (MW) Lewis acid sites as a function of the dopant concentration. The dashed vertical line corresponds to a group 1 metal salt concentration of 0.3 mmol $g_{(cat)}^{-1}$.

with the two doped catalysts displaying broadly similar profiles. The band at 3770 cm^{-1}, assigned to hydroxyl groups interacting with pyridine on medium-strong Lewis acid sites,[10] is attenuated rapidly. For CsCl, this feature is effectively lost at a dopant level of 0.1 mmol $g_{(cat)}^{-1}$, whereas in the case of KCl, a loading of ~0.3 mmol $g_{(cat)}^{-1}$ is required to achieve the same outcome, indicating the Cs salt to be more effective in neutralizing this particular site. Over the same loading range, there is no observed change in the band at 3730 cm^{-1} that is associated with medium-weak Lewis acid sites,[10] indicating that the modifier is selectively blocking stronger acid sites at lower loadings. Thereafter, on increasing the modifier concentration for both group 1 metal salts above 0.3 mmol $g_{(cat)}^{-1}$, the medium-weak site is rapidly quenched. It appears that the group 1 metal salt loading is preferentially removing the stronger Lewis acid sites of the η-alumina. Interestingly, whereas the intensity of the pyridine ν(C−C) 8a modes displays a discontinuous behavior with respect to modifier loading (Figures 2 and 4), the intensity profiles for the alumina ν(O−H) modes are effectively continuous (Figure 7). This contrast is thought to reflect the lower density of hydroxyl groups compared to that of the more close-range pyridine−metal salt interactions that give rise to the spectral intensities displayed in Figures 1 and 3.

The pyridine 8a mode trends presented in Figures 1 and 3 do not correlate with the deductions arrived at from the inspection of the ν(O−H) profiles of η-alumina (Figures 5−7). For both dopants, whereas Figure 7 shows attenuation of the medium-strong and medium-weak Lewis acid sites over the range of 0.3−1.0 mmol $g_{(cat)}^{-1}$, Figures 1 and 3 show that the pyridine 8a mode at 1613 cm^{-1}, assigned to medium-strength Lewis acid sites, remains visible up to the highest loading examined (1.0 mmol $g_{(cat)}^{-1}$). In the light of previous measurements involving thermal treatment of the reference alumina, which indicated good correlation between pyridine ν(C−C) and alumina ν(O−H) features,[10] the discrepancies evident between Figures 1/3 and 5/6 may indicate that there are additional surface chemical factors in play when group 1 metal salt modifiers are present. In an attempt to better understand factors contributing to the pyridine IR data, a series of temperature-programmed IR experiments were performed. These are described in the following section.

2.2. Temperature-Programmed IR Spectroscopy.

Further evaluation of the acid site distribution of the modified alumina catalysts was obtained from a series of temperature-programmed infrared measurements. Using this technique, alumina samples could be heated to induce the selective desorption of pyridine from specific Lewis acid sites. Previously reported pyridine TPD measurements revealed the desorption of the medium-strong and medium-weak Lewis acid sites to exhibit peak maxima at, respectively, 650 and 460 K,[10] while temperature-programmed IR measurements showed the strong Lewis acid site (1623 cm^{-1}) to remain populated on heating to temperatures of 823 K.[10] Specifically, the pyridine 8a mode at 1623 cm^{-1} lost only ~14% of its intensity on warming to 823 K at 8 K min^{-1}.[10]

Figures 8 and 9 show the infrared difference spectra obtained for pyridine adsorbed on the CsCl- and KCl-modified catalysts, respectively, after heating to 423 K. With reference to the previous work on the undoped reference η-alumina catalyst, this temperature corresponds to the desorption of the majority (~85%) of pyridine from the weak Lewis acid site,[10] effectively leaving pyridine in predominantly strong and medium-strength Lewis acid sites. Reducing the concentration of the weak Lewis acid site assists in resolving the distribution of pyridine 8a modes, making it clearer to discern how modifier loading is affecting different sites on the alumina surface. Figures 8 and 9 show that at low group 1 metal salt loadings, there are bands at 1623 and 1613 cm^{-1}, assigned to pyridine adsorbed on strong and medium-strength Lewis acid sites. On addition of 0.1 mmol $g_{(cat)}^{-1}$ of the group 1 metal salt modifier, the band at 1623 cm^{-1} is no longer present, indicating the complete removal of this site.

DOI: 10.1021/acsomega.9b01719
ACS Omega 2019, 4, 13981−13990

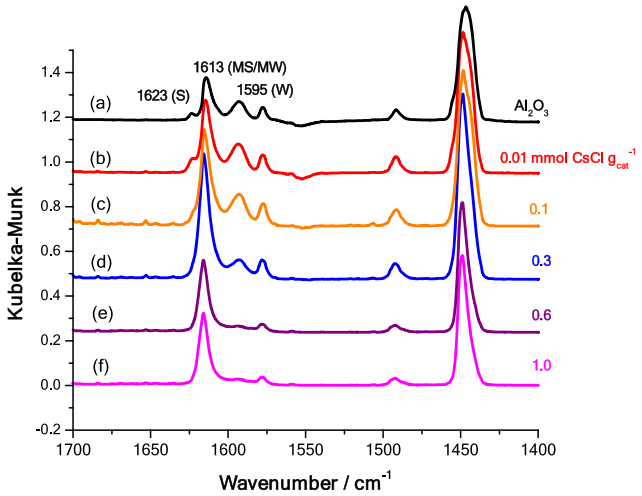

Figure 8. Infrared spectra of a saturated overlayer of pyridine heated to 423 K on a range of CsCl-doped alumina catalysts: (a) undoped η-alumina, (b) 0.01 mmol CsCl $g_{(alumina)}^{-1}$, (c) 0.1 mmol CsCl $g_{(alumina)}^{-1}$, (d) 0.3 mmol CsCl $g_{(alumina)}^{-1}$, (e) 0.6 mmol CsCl $g_{(alumina)}^{-1}$, and (f) 1.0 mmol CsCl $g_{(alumina)}^{-1}$. The spectra are offset for clarity.

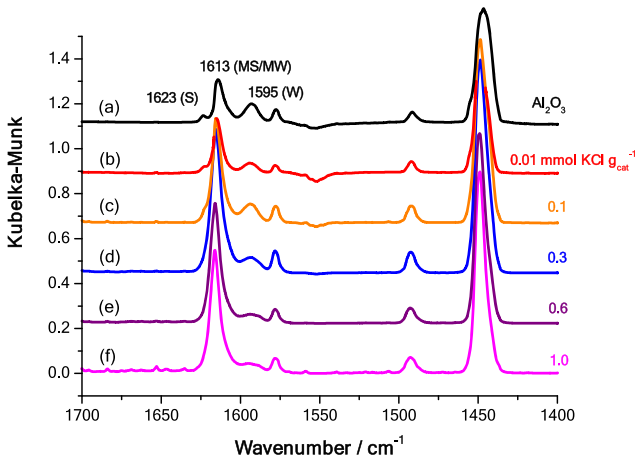

Figure 9. Infrared spectra of a saturated overlayer of pyridine heated to 423 K on a range of KCl-doped alumina catalysts: (a) undoped η-alumina, (b) 0.01 mmol KCl $g_{(cat)}^{-1}$, (c) 0.1 mmol KCl $g_{(cat)}^{-1}$, (d) 0.3 mmol KCl $g_{(cat)}^{-1}$, (e) 0.6 mmol KCl $g_{(cat)}^{-1}$, and (f) 1.0 mmol KCl $g_{(cat)}^{-1}$. The spectra are offset for clarity.

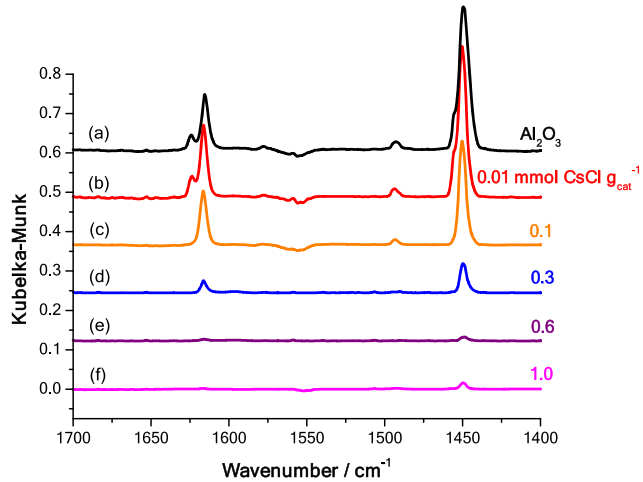

Figure 10. Infrared spectra obtained for a saturated overlayer of pyridine heated to 623 K for a range of CsCl-doped catalysts: (a) undoped η-alumina, (b) 0.01 mmol CsCl $g_{(cat)}^{-1}$, (c) 0.1 mmol CsCl $g_{(cat)}^{-1}$, (d) 0.3 mmol CsCl $g_{(cat)}^{-1}$, (e) 0.6 mmol CsCl $g_{(cat)}^{-1}$, and (f) 1.0 mmol CsCl $g_{(cat)}^{-1}$. The spectra are offset for clarity.

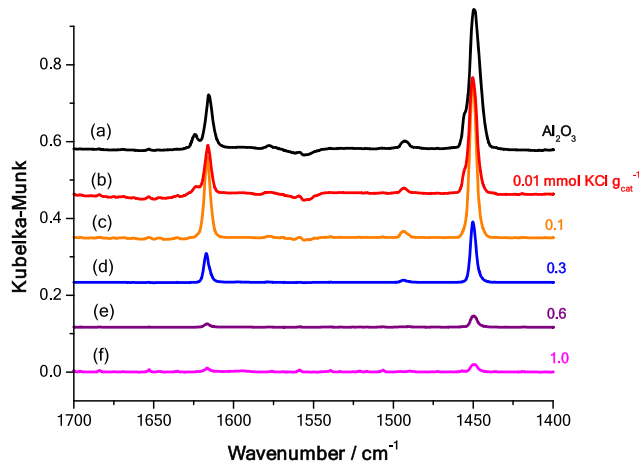

Figure 11. Infrared spectra obtained for a saturated overlayer of pyridine heated to 623 K for a range of KCl-doped catalysts: (a) undoped η-alumina, (b) 0.01 mmol KCl $g_{(cat)}^{-1}$, (c) 0.1 mmol KCl $g_{(cat)}^{-1}$, (d) 0.3 mmol KCl $g_{(cat)}^{-1}$, (e) 0.6 mmol KCl $g_{(cat)}^{-1}$, and (f) 1.0 mmol KCl $g_{(cat)}^{-1}$. The spectra are offset for clarity.

The spectra obtained at 423 K (Figures 8 and 9) do not readily allow the quantification of the effect of the modifiers on the medium-strength sites since pyridine remains adsorbed on both sites at this temperature. By increasing the desorption temperature to 623 K, only pyridine adsorbed on strong and medium-strong sites will remain due to complete desorption from the medium-weak site.[10] Figures 10 and 11 show the infrared spectra after pyridine desorption at 623 K for the CsCl- and KCl-modified catalysts, respectively. At low modifier loadings, pyridine 8a bands associated with strong (1623 cm^{-1}) and medium (1613 cm^{-1}) Lewis acid sites are observed. Concentrating on CsCl, Figure S1 presents the curve fitting of the pyridine 8a peaks observed in the diffuse reflectance infrared Fourier transform spectroscopy DRIFTS spectrum of the η-alumina +0.01 mmol CsCl $g_{(cat)}^{-1}$ sample (Figure 10b). Figure 12a presents the integrated intensity of the pyridine 8a modes observed in Figure 10. Increasing the modifier loading to 0.1 mmol $g_{(cat)}^{-1}$ results in the loss of the 8a mode associated with the strong Lewis acid site. Continued increases in the dopant loading lead to the attenuation and almost complete removal of the band at 1613 cm^{-1}, indicating the quenching of the medium site. Thus, these results indicate that a dopant loading of 0.1 mmol $g_{(cat)}^{-1}$ is required to completely "cap" the strong Lewis acid sites, while a loading of ~0.6 mmol $g_{(cat)}^{-1}$ is required to effectively remove medium-strong Lewis acid sites.

The clarity of the infrared spectra of the pyridine 8a mode in Figures 10 and 11 relative to that observed in Figures 1, 3, 8, and 9 is consistent with the possibility that, within a condensed pyridine overlayer in the presence of a coadsorbed group 1 metal chloride, dipole coupling is complicating spectral intensities. In this way, the heating of a pyridine-dosed sample to 623 K appears to minimize nearest-neighbor interactions, enabling pyridine spectral intensity to better correlate with the

DOI: 10.1021/acsomega.9b01719
ACS Omega 2019, 4, 13981−13990

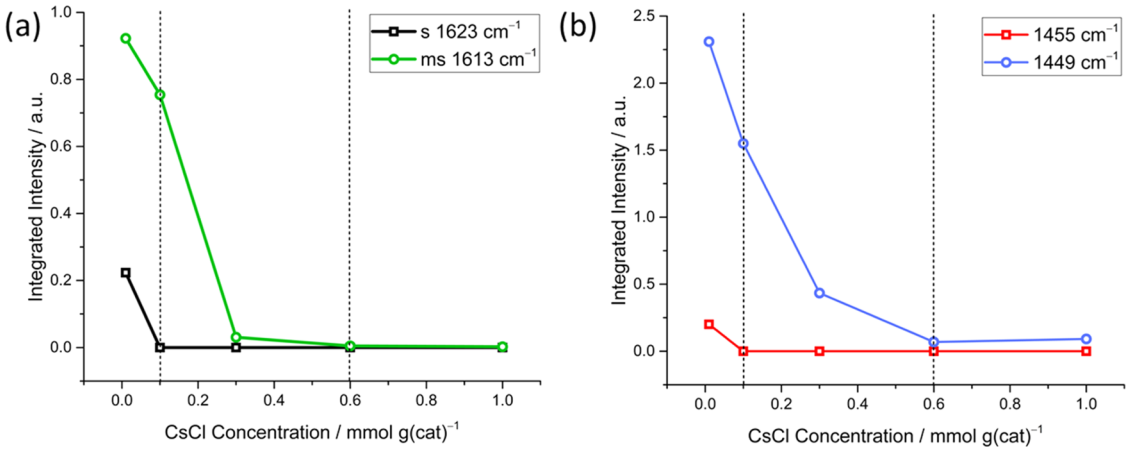

Figure 12. Integrated intensity of (a) the pyridine 8a peaks and (b) the pyridine 19b peaks observed in Figure 10 (saturated overlayer of pyridine heated to 623 K for CsCl-doped samples) as a function of CsCl concentration. Dashed vertical lines signify concentrations of 0.1 and 0.6 mmol CsCl $g_{(cat)}^{-1}$.

information contained within the ν(O−H) modes (e.g., Figure 7).

The differences between Figures 10 and 11 are modest, indicating that the two group 1 metal salts are operating in a similar manner. However, the spectra corresponding to a modifier loading of 0.3 mmol $g_{(cat)}^{-1}$ (Figures 10d and 11d) do show a greater attenuation of the medium-strength Lewis acid site for CsCl compared to that for KCl, a further indication that CsCl is a more effective neutralizing entity than KCl, possibly due to the larger size of the CsCl ion pair (Section 3). For completeness, it is noted that a weak feature at 1575 cm^{-1} is observed in Figures 10 and 11; this is assigned to the 8b mode of pyridine bonded to Lewis acid sites.[10]

The use of temperature-programmed infrared spectroscopy of a chemisorbed pyridine overlayer also provides the opportunity to correlate the pyridine 8a mode with that of the pyridine 19b mode. On the undoped alumina, Figure 10 shows the latter mode to be characterized by an intense peak centered at 1449 cm^{-1} that possesses a high wavenumber shoulder at ∼1455 cm^{-1}. Figure S2 presents the curve fitting of the pyridine 19b peaks observed in the DRIFTS spectrum of the η-alumina +0.01 mmol CsCl $g_{(cat)}^{-1}$ sample (Figure 10b). Figure 12b presents the integrated intensity of the pyridine 19b modes observed in Figure 10. At 0.1 mmol CsCl $g_{(cat)}^{-1}$, the shoulder completely disappears, leaving an attenuated symmetric band that is substantially diminished by 0.6 mmol CsCl $g_{(cat)}^{-1}$. Indeed, the profiles of Figure 12a,b are remarkably similar. In this way, the weaker feature in Figure 10 at 1455 cm^{-1} is assigned to pyridine adsorbed on strong Lewis acid sites, while the distinct band at 1449 cm^{-1} is attributed to pyridine at medium-strong Lewis acid sites. The following section uses mass-selective temperature-programmed desorption experiments of chemisorbed pyridine to further interrogate the feasibility of using group 1 chlorides to effect site-selective chemistry.

2.3. Temperature-Programmed Desorption. A series of pyridine temperature-programmed desorption (TPD) experiments were performed on the range of CsCl- and KCl-doped alumina catalysts. The results obtained from these measurements are shown in Figures 13 and 14. The standard alumina spectrum, used as a reference, shows two features corresponding to pyridine desorbing from medium-weak and medium-strong Lewis acid sites.[10] At low dopant loadings, the higher

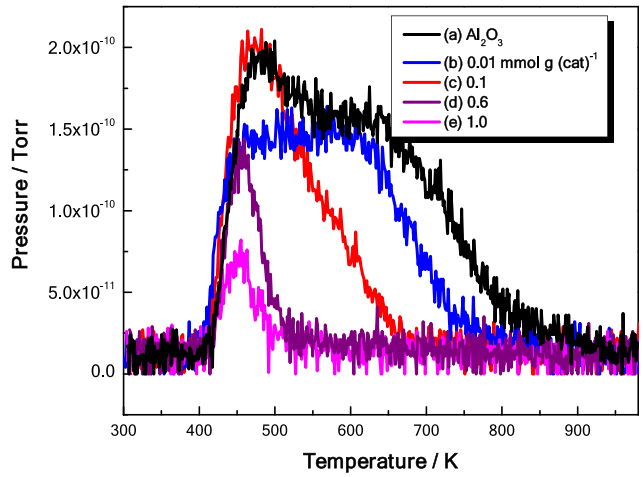

Figure 13. Pyridine TPD profiles obtained for a saturated chemisorbed dose on a range of CsCl-doped alumina catalysts: (a) undoped η-alumina, (b) 0.01 mmol CsCl $g_{(cat)}^{-1}$, (c) 0.1 mmol CsCl $g_{(cat)}^{-1}$, (d) 0.6 mmol CsCl $g_{(cat)}^{-1}$, and (e) 1.0 mmol CsCl $g_{(cat)}^{-1}$.

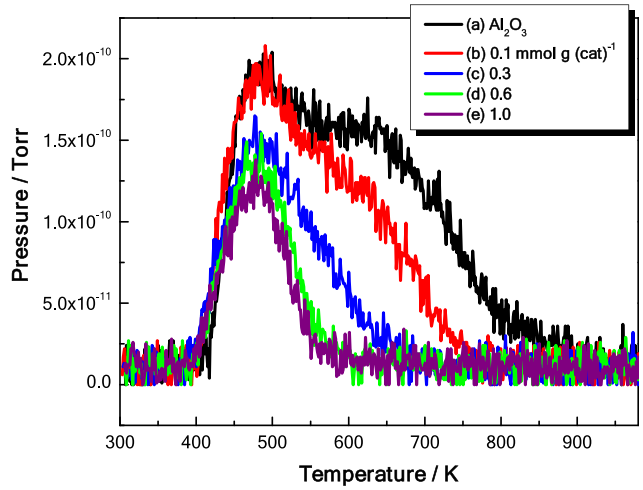

Figure 14. Pyridine TPD profiles obtained for a saturated chemisorbed dose on a range of KCl-doped alumina catalysts: (a) undoped η-alumina, (b) 0.1, (c) 0.3 mmol KCl $g_{(cat)}^{-1}$, (d) 0.6 mmol KCl $g_{(cat)}^{-1}$, and (e) 1.0 mmol KCl $g_{(cat)}^{-1}$.

DOI: 10.1021/acsomega.9b01719
ACS Omega 2019, 4, 13981−13990

temperature feature associated with the medium-strong Lewis acid site is gradually lost until by 0.6 mmol $g_{(cat)}^{-1}$ it is unobservable. This rather nicely shows the effect of increasing dopant loading on the medium-strong site and is entirely consistent with the temperature-programmed pyridine IR studies (Section 2.2). The low-temperature feature, assigned to the medium-weak Lewis acid sites,[10] remains essentially unaffected up to 0.3 mmol $g_{(cat)}^{-1}$, indicating that the medium-strong site is removed selectively by the addition of low concentrations of a modifier.

These trends are illustrated in Figure 15, which shows the integrated areas of the features associated with medium-strong

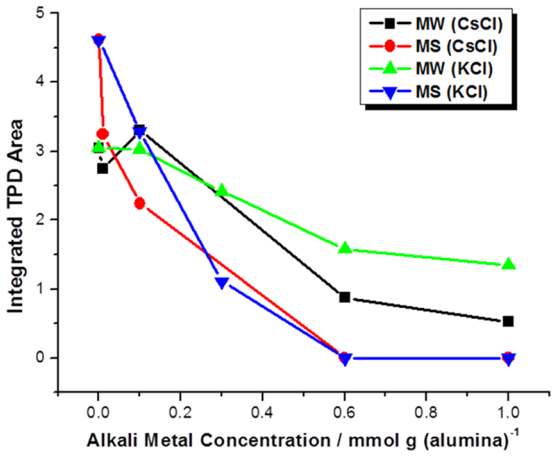

Figure 15. Integrated TPD areas for medium-strong (MS) and medium-weak (MW) Lewis acid sites as a function of group 1 metal salt modifier loading.

and medium-weak sites as a function of modifier loading. A loading of 0.3 mmol $g_{(cat)}^{-1}$ appears to mark the point above which it is possible to remove medium-weak sites, as above this level, a gradual decrease in the medium-weak feature is observed. Increasing modifier concentration up to 1.0 mmol $g_{(cat)}^{-1}$ results in a reduction of the medium-weak feature by ca. 50%. Together, the IR and TPD results describe a form of "titration" process, by which medium-strong sites are removed at low dopant loadings, followed by medium-weak sites as dopant concentrations are increased. Concentrating on the profile for the medium-weak site in Figure 15, CsCl is more effective in the neutralization of this site relative to its K counterpart.

3. DISCUSSION

A combination of infrared spectroscopy with temperature-programmed desorption studies has allowed an analysis of the effect of group 1 metal salt dopants on the Lewis acidity of reference transition alumina. It is recognized that there will be a degree of competitive adsorption between the different Lewis acid sites and the group 1 metal salt modifier. Nonetheless, the preceding data indicate a degree of quantization of adsorption as a function of modifier loading. Specifically, IR analysis of the alumina ν(O−H) modes provides information on the medium-strong and medium-weak Lewis acid sites (Figure 7); temperature-programmed IR analysis of pyridine 8a and 19b modes provides information on the strong and medium-strong Lewis acid sites (Figure 12); TPD experiments provide information on the medium-weak and medium-strong Lewis acid site populations (Figure 15). The temperature-programmed IR studies circumvent complications with pyridine 8a band intensities, and the additional analysis of the pyridine 19b mode is consistent with 8a-derived deductions, thereby signifying a high degree of internal consistency.

The resulting deductions are outlined in Table 1, which summarizes the Lewis acid site distribution at the η-alumina

Table 1. Lewis Acid Site Distribution at the η-Alumina Surface After the Addition of Varying Concentrations of KCl and CsCl Dopants

group 1 metal salt loading (mmol $g_{(cat)}^{-1}$)	Lewis acid sites present at the surface
0	strong, medium-strong, medium-weak, weak
0.01	strong, medium-strong, medium-weak, weak
0.1	medium-strong, medium-weak, weak
0.3	medium-strong, medium-weak, weak
0.6	medium-weak, weak
1.0	medium-weak, weak

surface after the addition of varying concentrations of dopants. Although Section 2 shows broadly consistent trends when using the two different alkali metal chloride modifiers, Figures 7 and 15 indicate that the effect is slighter greater for CsCl compared with that for KCl.

The perspective gleaned from this analysis of the surface Lewis acid site distribution of η-alumina as a function of modifier loading is illustrated schematically in Figure 16. As considered previously,[10] the clean activated η-alumina surface is composed of (i) strong, (ii) medium-strong, (iii) medium-weak, and (iv) weak Lewis acid sites; this situation is represented by Figure 16a. Concentrating on CsCl as a representative dopant and considering the case for a high dopant coverage (1.0 mmol CsCl $g_{(cat)}^{-1}$), Figure 16b shows the modifier to have completely neutralized the strong and medium-strong Lewis acid sites while partially reducing the density of medium-weak Lewis acid sites. Thus, the active surface of a group 1 metal chloride-doped η-alumina is composed of weak Lewis acid sites and a reduced population of medium-weak Lewis acid sites. It is the combination of sites presented in Figure 16b that defines the active phase of a group 1 metal salt-doped η-alumina catalyst that conveys acceptable rates of methyl chloride formation and negligible rates of dimethyl ether production. While it is acknowledged that this spectroscopic investigation demonstrates fair coherence to the titration concept where group 1 metal salts can affect site-selective chemistry, this study is inherently limited to internal validation. However, external validation for the trends outlined here is evidenced by the enhanced catalytic performance recently reported for this new generation of a methyl chloride synthesis catalyst.[17]

Finally, we briefly consider possible origins for the differences induced by KCl and CsCl dopings. Previous work by Baird et al. has reported on interactions between cesium and potassium fluoride islands on γ alumina, which considers a role for ion pairs in the surface chemistry, i.e., K^+F^- or Cs^+F^-.[22] It is possible that the CsCl and KCl dopants considered in the present study are present at the surface as ion-pair islands. This scenario then leads to possibilities of how differences in the cation, e.g., cation size and consequent interionic difference, may influence base activity. KCl adopts the face-centered cubic rock salt structure (a = 6.2931 Å),

DOI: 10.1021/acsomega.9b01719
ACS Omega 2019, 4, 13981−13990

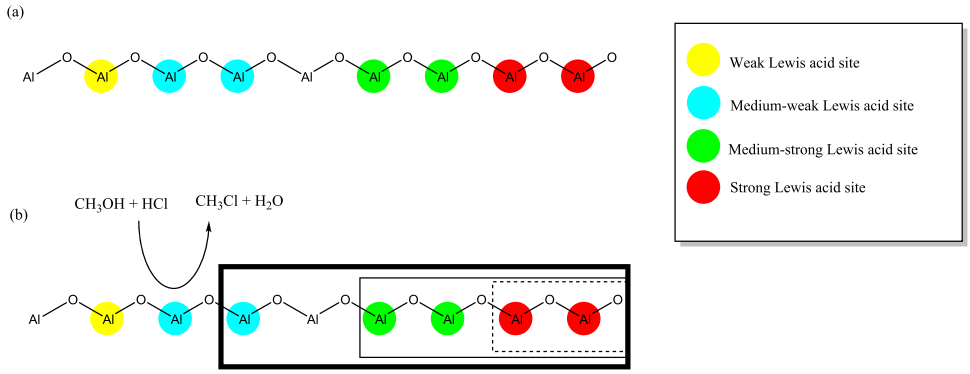

Figure 16. Schematic representation of (a) an activated η-alumina surface and (b) η-alumina doped with varying levels of CsCl modifier. The dashed line corresponds to a dopant level of 0.1 mmol CsCl $g_{(cat)}^{-1}$ that neutralizes the strong Lewis acid sites; the thin solid line corresponds to a dopant level of 0.6 mmol CsCl $g_{(cat)}^{-1}$ that neutralizes the strong and medium-strong Lewis acid sites; the thick solid line corresponds to a dopant level of 1.0 mmol CsCl $g_{(cat)}^{-1}$ that neutralizes the strong and medium-strong Lewis acid sites and a proportion of the medium-weak Lewis acid sites.

whereas CsCl adopts a simple cubic structure (a = 4.123 Å).[23] Thus, it is possible that the consistently more potent attenuation of Lewis acid sites of CsCl compared to that of KCl, as evidenced in Figures 7 and 15, could be a reflection of the local structure of the two modifiers. This suggestion is speculative and constitutes a topic worthy of further investigation.

4. CONCLUSIONS

This work has used a combination of pyridine chemisorption coupled to infrared spectroscopy and temperature-programmed desorption measurements to examine how the addition of group 1 metal chlorides can modify the acid site distribution of an η-alumina catalyst. The following conclusions can be drawn:

- A group 1 metal chloride loading of 0.1 mmol $g_{(cat)}^{-1}$ is sufficient to neutralize the strong Lewis acid sites. Figures 1, 3, 8, and 9 justify this statement.
- A group 1 metal chloride loading of 0.6 mmol $g_{(cat)}^{-1}$ is sufficient to neutralize the strong and medium-strong Lewis acid sites. Figures 7, 10, 11, and 15 justify this statement.
- A group 1 metal chloride loading of 1.0 mmol $g_{(cat)}^{-1}$ neutralizes the strong and medium-strong Lewis acid sites and partially neutralizes the medium-weak Lewis acid site. Figures 13, 14, and 15 justify this statement.
- The loading of a group 1 metal chloride can act as a titrant that enables selective neutralization of the distribution of Lewis acid sites present at the surface of an η-alumina catalyst.
- At a group 1 metal chloride loading of 1.0 mmol $g_{(cat)}^{-1}$, the surface is characterized by a distribution of medium-weak and weak Lewis acid sites; these sites define the active phase of a methyl chloride synthesis catalysis that is highly selective to methyl chloride production. Figure 16b presents a schematic illustration of the η-alumina surface during this phase of operation.

5. EXPERIMENTAL SECTION

5.1. Catalyst Preparation. The η-alumina reference catalyst was supplied by Ineos Chlor (Ineos Chlor catalyst ref: 25867); this is the same transition alumina examined in the previous studies[11−14] and has been comprehensively characterized elsewhere.[10] The doping of the alumina catalyst with K and Cs salts was performed by an impregnation method. An aqueous solution of CsCl (Sigma-Aldrich, purity 99.9%) or KCl (Sigma-Aldrich, purity 99.999%) of precalculated concentration was added to a Pyrex flask via a two-way adaptor and a dropping funnel while under vacuum (<10^{-2} Torr). The use of an evacuated vessel ensured that the salt solution entered and filled the pores of the alumina in a uniform fashion. The solution was decanted to remove excess liquid, and the catalyst was dried by rotary evaporation at 343 K for 2 h, before final drying in an oven at 353 K for a further 2 h. Varying the concentration of the original salt solution enabled the base η-alumina catalyst to be prepared with a range of group 1 metal salt dopant concentrations. As an indication for how the dopant loading affects the structure/porosity of the alumina, Table 2 provides the surface area and pore volume values for the reference catalyst and five CsCl-doped samples (0.01−1.0 mmol CsCl $g_{(cat)}^{-1}$).

Table 2. BET Surface Analysis for the Five CsCl-Doped η-Alumina Catalysts[a]

CsCl-doped catalysts (mmol CsCl $g_{(cat)}^{-1}$)	BET surface area (m^2 g^{-1})	pore volume (cm^3 g^{-1})
0	270 ± 4	0.30 ± 0.005
0.01	259 ± 5	0.29 ± 0.006
0.1	248 ± 5	0.27 ± 0.004
0.3	232 ± 2	0.25 ± 0.005
0.6	186 ± 6	0.19 ± 0.006
1.0	139 ± 3	0.16 ± 0.003

[a]Results for the η-alumina reference catalyst are additionally included. Errors represent the standard deviation from three replicate measurements.

Table 2 shows that increasing CsCl loadings lead to reductions in the total surface area, as well as pore volume.

5.2. Infrared Spectroscopy. Infrared experiments were performed using a Nicolet Nexus Fourier transform infrared spectrometer fitted with an MCT high D* detector. Measurements were performed in diffuse reflectance mode using a SpectraTech Smart diffuse reflectance cell and environmental chamber, using a typical sample size of 50 mg of the catalyst. Background spectra were recorded post activation at 293 K. Pyridine was dosed onto the catalyst at 373 K using pulse-flow

DOI: 10.1021/acsomega.9b01719
ACS Omega 2019, 4, 13981−13990

techniques. The elevated temperature prevented the retention of physisorbed pyridine and resulted in a chemisorbed layer on alumina. After dosing, the sample temperature was allowed to cool to 293 K and then the spectrum was recorded (128 scans, resolution 2 cm^{-1}). All spectra are presented as background subtractions, where a spectrum of the activated catalyst has been subtracted from the dosed catalyst spectrum. No baseline or offset corrections were made. For pyridine desorption experiments, the cell containing alumina, previously dosed with pyridine as above, was heated under flowing He. The cell was maintained at each temperature for 15 min and allowed to cool down to room temperature, and then a spectrum was recorded. The alumina is retained in the η-phase under these conditions. Infrared peak areas were determined using a Gaussian fitting function available within the Origin graphical software package.

5.3. Temperature-Programmed Desorption. Thermal desorption experiments were performed with the catalyst sample (ca. 0.1 g) contained within a packed bed tubular reactor (1/4 in. stainless steel tubing) located within a temperature-programmable oven (Neytech 25 PAF). A mass spectrometer (Leda Mass Gas Analyzer, LM22, closed-ion source) sampled the eluting gases via a differentially pumped capillary line and a metal-sintered precision leak. The alumina sample was activated and dosed with pyridine as outlined above, using high-purity helium as the carrier gas. Saturation of the sample could be observed by monitoring the pyridine breakthrough in the eluent stream on the mass spectrometer. When saturation was achieved, the sample was left to purge overnight at 373 K under a flowing He. This resulted in the selective desorption of weakly bound pyridine.[10] Temperature-programmed desorption (TPD) runs were carried out using the temperature-programmable oven, set at a heating rate of 8 K min^{-1}. The eluent stream from the reactor was monitored by the mass spectrometer at all times during the TPD experiment. To ensure the rapid transition of desorbing species through the mass spectrometer pumping system, the split valve for the elutant feedline into the mass spectrometer was set such that the majority of the desorbing gases were passed to the vent. While this arrangement facilitates good peak resolution in the TPD profiles, it does lead to relatively low signal : noise ratio plots. All IR and TPD measurements have been performed at least in duplicate, with the profiles presented here being representative of the observed trends.

■ ASSOCIATED CONTENT

Supporting Information

The Supporting Information is available free of charge on the ACS Publications website at DOI: 10.1021/acsomega.9b01719.

> Curve fitting of the pyridine 8a mode for the DRIFTS spectrum of a saturated overlayer of pyridine on η-alumina + 0.01 mmol CsCl $g_{(cat)}^{-1}$ that has been heated to 623 K (Figure S1); and curve fitting of the pyridine 19b mode for the DRIFTS spectrum of a saturated overlayer of pyridine on η-alumina +0.01 mmol CsCl $g_{(cat)}^{-1}$ that has been heated to 623 K (Figure S2) (PDF)

■ AUTHOR INFORMATION

Corresponding Author

*E-mail: David.Lennon@glasgow.ac.uk. Tel: +44-141-330-4372.

ORCID

David Lennon: 0000-0001-8397-0528

Notes

The authors declare no competing financial interest.

■ ACKNOWLEDGMENTS

The EPSRC (grant number GR/P01984/01) and Ineos Chlor are thanked for project support and the provision of an Industrial CASE award (ARM).

■ REFERENCES

(1) Weissermel, K.; Arpe, H.-J. *Industrial Organic Chemistry*, 4th ed.; Wiley-VCH: Weinheim, 2003; pp 52−57.

(2) Market Research Future, Chloromethane Market Research Report—Forecast to 2022, May 2019. https://www.marketresearchfuture.com/reports/chloromethane-market-2417 (accessed July 05, 2019).

(3) Lennon, D.; Winfield, J. M. In *New Materials for Catalytic Applications*; Kemnitz, E.; Parvulescu, V. Eds.; Elsevier: Amsterdam, 2016, Chapter 7, ISBN 9780444635877.

(4) Schmidt, S. A.; Kumar, N.; Zhang, B.; Eränen, K.; Murzin, D. Y.; Salmi, T. Preparation and Characterization of Alumina-Based Microreactors for Application in Methyl Chloride Synthesis. *Ind. Eng. Chem. Res.* **2012**, *51*, 4545−4555.

(5) Schmidt, S. A.; Kumar, N.; Reinsdorf, A.; Eränen, K.; Wärnå, J.; Murzin, D. Y.; Salmi, T. Methyl chloride synthesis over Al_2O_3 catalyst coated microstructured reactor-Thermodynamics, kinetics and mass transfer. *Chem. Eng. Sci.* **2013**, *95*, 232−245.

(6) Schmidt, S. A.; Kumar, N.; Shchukarev, A.; Eränen, K.; Mikkola, J.-P.; Murzin, D. Y.; Salmi, T. Preparation and characterization of neat and $ZnCl_2$ modified zeolites and alumina for methyl chloride synthesis. *Appl. Catal., A* **2013**, *468*, 120−134.

(7) Schmidt, S. A.; Peurla, M.; Kumar, N.; Eränen, K.; Murzin, D. Y.; Salmi, T. Preparation of selective $ZnCl_2$/alumina catalysts for methyl chloride synthesis: Influence of pH, precursor and zinc loading. *Appl. Catal., A* **2015**, *490*, 117−127.

(8) Lundie, D. T. Investigation of the Active Sites on Methyl Chloride Synthesis Catalysts. Ph.D. Thesis, University of Glasgow, 2003.

(9) McInroy, A. R. Investigation of a New Generation of Methyl Chloride Synthesis Catalysts. Ph.D. Thesis, University of Glasgow, 2006.

(10) Lundie, D. T.; McInroy, A. R.; Marshall, R.; Winfield, J. M.; Jones, P.; Dudman, C. C.; Parker, S. F.; Mitchell, C. J.; Lennon, D. An improved description of the surface acidity of η-alumina. *J. Phys. Chem. B* **2005**, *109*, 11592−11601.

(11) McInroy, A. R.; Lundie, D. T.; Winfield, J. M.; Dudman, C. C.; Jones, P.; Parker, S. F.; Taylor, J. W.; Lennon, D. An infrared and inelastic neutron scattering spectroscopic investigation on the interaction of η-alumina and methanol. *Phys. .Chem. Chem. Phys.* **2005**, *7*, 3093−3101.

(12) McInroy, A. R.; Lundie, D. T.; Winfield, J. M.; Dudman, C. C.; Jones, P.; Lennon, D. The application of diffuse reflectance infrared spectroscopy and temperature programmed desorption to investigate the interaction of methanol on η-alumina. *Langmuir* **2005**, *21*, 11092−11098.

(13) McInroy, A. R.; Lundie, D. T.; Winfield, J. M.; Dudman, C. C.; Jones, P.; Parker, S. F.; Lennon, D. The interaction of alumina with HCl: an infrared spectroscopy and inelastic neutron scattering study. *Catal. Today* **2006**, *114*, 403−411.

(14) McInroy, A. R.; Lundie, D. T.; Winfield, J. M.; Jones, P.; Dudman, C. C.; Lennon, D. Improved atom efficiency via an appreciation of the surface activity of alumina catalysts: methyl chloride synthesis. *Appl. Catal., B* **2007**, *70*, 606−610.

(15) Parker, S. F.; Lennon, D. Inelastic Neutron Scattering Studies of Methyl Chloride Synthesis over Alumina. *Acc. Chem. Res.* **2014**, *47*, 1220−1227.

(16) Lennon, D.; Winfield, J. M. Nano-sized Metal Fluorides: Novel Approaches to Lewis Acid Catalysts. *Molecules* **2017**, *22*, 201.
(17) McInroy, A. R.; Winfield, J. M.; Dudman, C. C.; Jones, P.; Lennon, D. The development of a new generation of methyl chloride synthesis catalyst. *Faraday Discuss.* **2016**, *188*, 467−479.
(18) Busca, G. The surface of transitional aluminas: A critical review. *Catal. Today* **2014**, *226*, 2−13.
(19) Morterra, C.; Chiorino, A.; Ghiotti, G.; Garrone, E. Surface-acidity of eta-alumina. 1. Pyridine chemisorption at room-temperature. *J. Chem. Soc., Faraday Trans.* **1979**, *75*, 271−288.
(20) Morterra, C.; Chiorino, A.; Ghiotti, G.; Garrone, E. Surface-acidity of eta-alumina. 2. Interaction of pyridine with other adsorbates. *J. Chem. Soc., Faraday Trans.* **1979**, *75*, 289−304.
(21) Anastas, P. T.; Kirchoff, M. M.; Williamson, T. C. Catalysis as a foundational pillar of green chemistry. *Appl. Catal., A* **2001**, *221*, 3−13.
(22) Baird, T.; Bendada, A.; Webb, G.; Winfield, J. M. Radiotracers in fluorine chemistry .17. Cesium and potassium fluorides supported on fluorinated gamma-alumina. *J. Fluorine Chem.* **1994**, *66*, 117−122.
(23) West, A. R. *Basic Solid State Chemistry*, 2nd ed.; Wiley: Chichester, 1999; pp 37 and 47.

DOI: 10.1021/acsomega.9b01719
ACS Omega 2019, 4, 13981−13990